http://dx.doi.org/10.5012/bkcs.2012.33.12.3981

Effect of Microwave Irradiation on Morphology and Size of Anatase Nano Powder: Efficient Photodegradation of 4-Nitrophenol by W-doped Titania

Abdollah Fallah Shojaei and Mohammad Hassan Loghmani*

*Department of Chemistry, Faculty of Science, University of Guilan, P.O. Box 1914, Rasht, Iran. *E-mail: chemlogh@gmail.com*
Received July 12, 2012, Accepted September 5, 2012

Anatase nanocrystalline and its tungsten-doped (0.4, 2, and 4 mol %) powders have been synthesized by microwave irradiation through hydrolysis of titanium tetra-isopropoxide (TIP) in aqueous solution. The materials are characterized by XRD, Raman, SEM-EDX, TEM, FT-IR and UV-vis techniques. The nanocrystalline TiO_2 particles are 30 nm in nature and doping of tungsten ion decreases their size. As seen in TEM images, the crystallites of W (4 mol %) doped TiO_2 are small with a size of about 10 nm. The photocatalytic activity was tested on the degradation of 4-nitrophenol (4-NP). Catalytic activities of W-doped and pure TiO_2 were also compared. The results show that the photocatalytic activity of the W-doped TiO_2 photocatalyst is much higher than that of pure TiO_2. Degradation decreases from 96 to 50%, during 115 min, when the initial 4-NP concentration increases from 10 to120 ppm. Maximum degradation was obtained at 35 mg of photocatalyst.

Key Words : Microwave, Anatase TiO_2, Nanocrystalline, Photocatalyst

Introduction

TiO_2 has been extensively studied as a kind of efficient photocatalyst for its excellent properties, such as non-toxicity, high thermal stability and low cost.[1,2] Titanium dioxide is in three different forms of rutile, anatase, and brookite.[3] At high temperatures, anatase and brookite can be irreversibly transformed to rutile phase.[4] Among the various polymorphs listed above, anatase was found to be photocatalytically more active than the others.[5] Nitrophenols are common pollutants in many natural water and wastewater systems. The mineralization of wastewaters contaminated by nitrophenols is extremely difficult in traditional methods, since nitrophenols are too stable in water. Based on hydroxyl radicals ($^{\bullet}OH$) photogeneration on TiO_2 surface, degradation of 4-NP can be alternated by UV irradiation. A number of methods have been used to prepare TiO_2 nanoparticles, such as chemical precipitation,[6] microemulsion-mediated hydrothermal,[7] hydrothermal crystallization,[8-10] sol-gel,[11] *etc*. Hole-electron recombination is a serious problem for the development of photocatalytically based technologies, since it severely limits the achievable quantum yields.[12] However, there are some strategies to reduce electron-hole recombination rates and increase photocatalyst efficiency. A common method consists of the doping of titania with transition metal ions while maintaining a good control of the primary particle size to achieve nanoscale configurations of the catalysts.[13,14] There are several reports in the literature of TiO_2 powder preparation by microwave processing. Yamamoto *et al.* studied hydrolysis and polycondensation of TIP in alkanediol solvent under microwave irradiation to obtain anatase TiO_2 nanocrystallite.[15] Hart *et al.* synthesized anatase TiO_2 by a sol-gel method followed by microwave heat treatment (silicon carbide was used as a microwave susceptor).[16] Also, Komarneni *et al.* reported microwave-hydrothermal synthesis of titanium dioxide under various reaction conditions.[17] In comparison with the other methods, microwave synthesis has the advantages of shortening the reaction time, giving products with small particle size, narrow size distribution and high purity. Tian[18] synthesized anatase W-TiO_2 by a hydrothermal method followed by $Ti(SO_4)_2$ and Na_2WO_4 as starting materials. In continuation of our group research on the synthesis and application of anatase nano scale,[19-22] we employed microwave process following the sol step to prepare the W-TiO_2 nanocrystallite. In addition, the purpose of the present work is to enlarge the photocatalytic activity of the TiO_2 by doping tungsten ions into anatase which shows very high photocatalytic efficiency. Water has a very high dipole moment which makes it one of the best solvents for microwave-assisted reactions. Therefore, the synthesis of pure and W-TiO_2 were carried out in the aqueous medium. W^{6+} is considered an interesting dopant of titania because it is believed that W^{6+} with small radius can be incorporated in the lattice of TiO_2. In most cases, nucleation and growth of nanoparticles are allowed to take place at a moderate temperature over an extended period of time, yielding a wide range of sizes. Thus, during a short time homogeneous heating of precursor has been used to achieve a narrow distribution of sizes by controlled microwave heating. The preparation of nano doped TiO_2 was carried out in the presence of acetic acid. Indeed, the excess acetate anion could also suppress the growth of TiO_2. This type of complexation of acetate anion on the surface of anatase form of TiO_2 might be responsible for the decrease in the crystallite size of TiO_2 during the synthesis. In order to have a transparent and homogenized sol, acetic acid was used before microwave heating. The synthesized TiO_2 was characterized by different analytical techniques such as XRD, Raman, SEM-EDX,

TEM and FT-IR. Then the photocatalytic activity of pure and W-doped TiO_2 was evaluated towards the degradation of 4-NP as model reactions.

Experimental

All the chemicals were obtained from Merck and used as such without further purification. The reagents employed were titanium(IV) isopropoxide, as a TiO_2 source; glacial acetic acid, as a catalyst; $Na_2WO_4{\cdot}2H_2O$, as dopant and water as a hydrolysis agent.

Synthesis of Titanium Dioxide. Anatase TiO_2 nanocrystalline were prepared by means of microwave heating. In this method, 8 mL titanium isopropoxide was initially added to 15.5 mL glacial acetic acid with stirring. Next, 170 mL deionized water was added to the mixture dropwise with vigorous stirring. The solution was stirred for 1 h to get a clear transparent sol. Finally, the sol was placed under microwave (Galanz, 2.45 GHz, 800w) irradiation (40% power) for 6 minutes. The white gel product was filtered, washed with deionized water and dried in oven for several hours. It was then calcined at 500 ºC in air for 5 h at a ramp rate of 5 ºC/min. To prepare W-doped TiO_2, the above procedure was repeated, including $Na_2WO_4{\cdot}2H_2O$ (0.4, 2, and 4 mol %) while adding water to the titanium isopropoxide mixture.

Characterization. X-ray diffraction (XRD) patterns were recorded by a D8 Bruker Advanced, X-ray diffractometer using Cu Kα radiation ($\lambda = 1.54$ Å). The patterns were collected in the range of 20-80º 2θ and continuous scan mode. The compositional analysis was done by energy dispersive X-ray. Scanning electron microscopy (SEM) images were obtained on Philips XL30 equipped with an energy dispersive X-ray spectroscopy. Transmission electron microscope (TEM) images were obtained on a Philips CM10 transmission electron microscope with an accelerating voltage of 100 kV. Fourier transform infrared (FT-IR) spectra were recorded on SHIMADZU 8800 spectrophotometer in KBr pellets. Raman spectra were recorded on Almega Thermo Nicolet dispersive spectrometer. An Nd:Y laser was used as an excitation source with 532 nm wavelength.

Photodegradation of 4-NP. The photocatalytic activity was tested on the degradation of 4-NP. The light was provided by a 400W high pressure Hg lamp without filter which was placed vertically in the reactor. The temperature of photodegradation system was adjusted by a water bath in which heating or cooling water recirculated through the jacket of the beaker. Prior to illumination, the reaction suspension was stirred continuously in dark for 30 minutes to ensure adsorption/desorption equilibrium. The suspension was magnetically stirred and bubbled with pure oxygen gas. After filtration, the concentration of 4-NP was determined by measuring its absorption by means of a RAYLEIGH (UV-1800) ultraviolet-visible (UV-vis) scanning spectrometer.

Results and Discussion

X-ray Diffraction (XRD) Studies. XRD patterns of various samples synthesized in the present investigation are shown in Figure 1. The XRD pattern corresponding to pure TiO_2, Figure 1(a) was found to match with that of anatase phase (JCPDS No. 4-477). All of the W-doped samples also exhibit XRD pattern matching with single phasic anatase, with JCPDS No. 2-406. However, no peaks from any other impurities were observed, which indicate the high purity of the obtained pure and W-doped TiO_2. The peaks corresponding to oxides of tungsten were not observed even for 4 mol % substituted samples. Therefore, pure TiO_2 and the W substituted samples on calcinations at 500 ºC for 5 h were found to retain anatase phase with no phase separation leading to rutile or WO_3 phase. Based on this, it can be inferred that either the entire tungsten has been substituted into the crystal lattice sites of the titania or it exists as WO_3 in a highly dispersed polymeric form over the titania surface. Since the ion radius of W^{n+} (0.62-0.70 Å) and Ti^{4+} (0.68 Å) are quite similar, it can be concluded that some Ti^{4+} in the lattice of TiO_2 are substituted by W^{n+} ($4 < n < 6$). The formation of Ti-O-W inhibits the transition of TiO_2 phase and blocks the Ti-O species at the interface with TiO_2 domains stabilizing them, thus preventing the agglomeration of TiO_2 nanoparticles and thus preventing the rutile growth.[23] There is also no discernible shift in the position of XRD lines with increasing extent of W-doping. The sharp diffraction peaks manifest that the obtained TiO_2 nano powders have high crystallinity. Compared to the commercial titania sample, the XRD peaks of all synthesized samples, pure and W-doped nano TiO_2, exhibit significant peak broadening, indicating smaller particle size. The average particle size was estimated by applying the Scherrer formula on the anatase (101) diffraction peak (the most intense peak): $D = K\lambda/\beta\cos\theta$, where D is the crystal size of the catalyst, λ the X-ray wavelength (1.54 Å), β the full width at half maximum

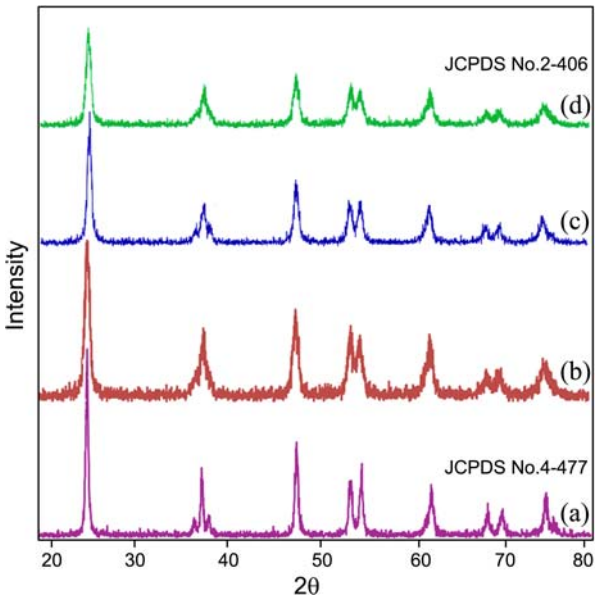

Figure 1. XRD pattern of TiO_2 calcined at 500 ºC (a) pure nano TiO_2, (b) 0.4% W-doped, (c) 2% W-doped, and (d) 4% W-doped nano TiO_2.

Table 1. Details, size and band gap of the all samples

Samples	XRD[a]	TEM[b]	B.G (eV):1240/λ
Pure	30 nm	30 nm	3.26
0.4% W-TiO_2	24 nm	25 nm	3.44
2.0% W-TiO_2	15 nm	15 nm	3.64
4.0% W-TiO_2	12 nm	10 nm	3.70

[a]Estimated by means of the Scherrers equation from broadening of (101) anatase reflection. [b]Estimated by direct measuring the particle size on the TEM images.

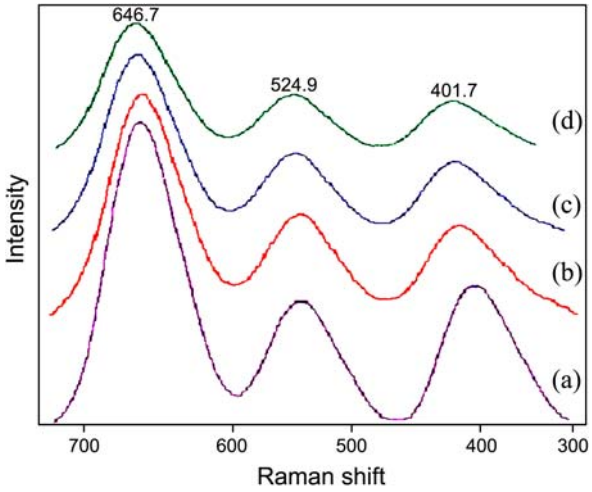

Figure 2. Raman spectra of TiO_2 calcined at 500 ºC (a) pure nano TiO_2, (b) 0.4% W-doped, (c) 2% W-doped, and (d) 4% W-doped nano TiO_2.

(FWHM) of the catalysts, $K = 0.89$ and θ is the diffraction angle. The details of the samples are summarized in Table 1.

Raman Spectroscopy. Optical Raman spectroscopy is a powerful tool in the study of TiO_2 for its high sensitivity to the microstructure. The spectra consist of three peaks. All the samples exhibit Raman bands around 401, 524 and 646 cm^{-1}, as shown in Figure 2. The bands at 401 and 524 cm^{-1} are assigned to B_{1g} and that at 646 cm^{-1} is assigned to E_g mode of vibrations of anatase titania phase.[24,25] Within the used wavelength in Raman analysis the peak related to the most intensive Eg Raman mode of anatase, at about 144 cm^{-1} was not observed. Absence of Raman bands (235, 447 and 612 cm^{-1}) corresponding to rutile phase of titania, again confirms the phase purity of these samples.[26] No bands are observed at 270, 293, 324, 715 and 807 cm^{-1}, which unequivocally establish the absence of separate WO_3 phase.[27] These results indicate that W does not exist as a separate crystalline oxide phase and must be incorporated in the crystal lattice of TiO_2. There is also a significant decrease in the intensity of the Raman bands with an increase in the doping concentration of the W in the TiO_2 crystal lattice. Thus the Raman spectroscopy data, in conjunction with XRD results establish the incorporation of W in the lattice of TiO_2.

SEM and TEM Micrographs. Morphology of the pure and doped TiO_2 was determined by SEM micrographs. SEM

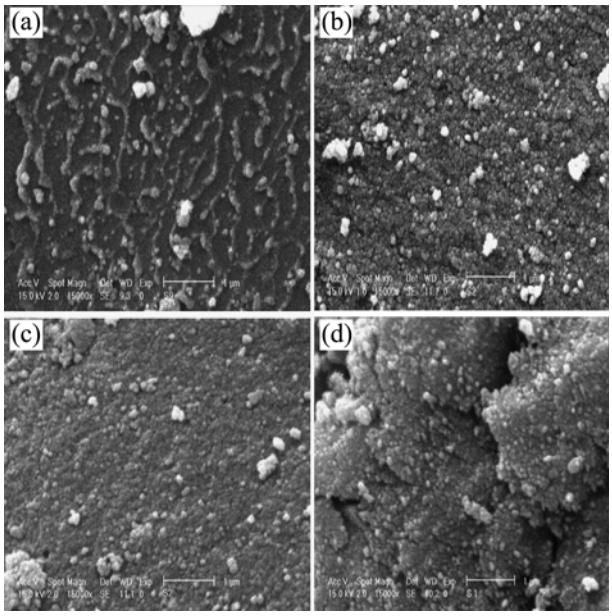

Figure 3. SEM images of TiO_2 (a) pure, (b) 0.4% W-doped, (c) 2% W-doped, and (d) 4% W-doped nano TiO_2.

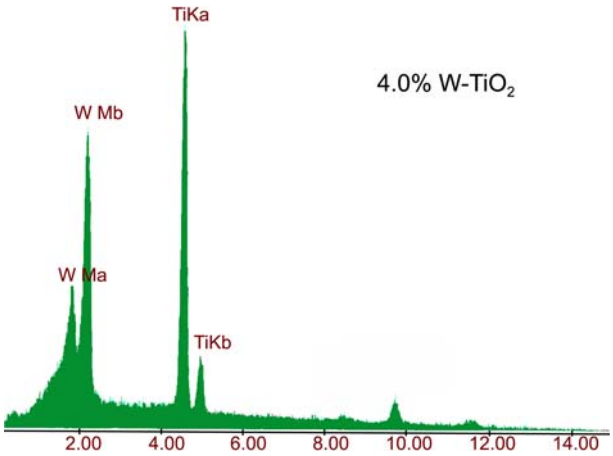

Figure 4. EDX pattern of 4% W-doped TiO_2.

micrographs of pure and W-doped nano TiO_2 are shown in Figure 3. It can be seen that, an increase in doping tungsten leads to a smaller TiO_2 particle; it is also observed that nano TiO_2 are in pseudospherical shapes. All samples present strong agglomeration when they are seen by SEM, the morphology and particle size of them cannot be resolved using this technique. The EDX data of W (4% mol)-doped TiO_2 is shown in Figure 4. Nano TiO_2 shows an intense peak around 4.5 keV. There are some tungsten peaks in the EDX pattern and this observation gave convincing evidence for the presence of tungsten on the surface of TiO_2. Figure 5 displays transmission electron micrographs (TEM) of 0, 0.4, 2, and 4 mol % nanocrystalline TiO_2 of size ~30, 25, 15 and 10 nm, respectively. It is observed from Figure 5 that there is a significant decrease in the size of the nano powders with an increase in doping tungsten ion. Therefore, this result may be attributed to the presence of tungsten component in the

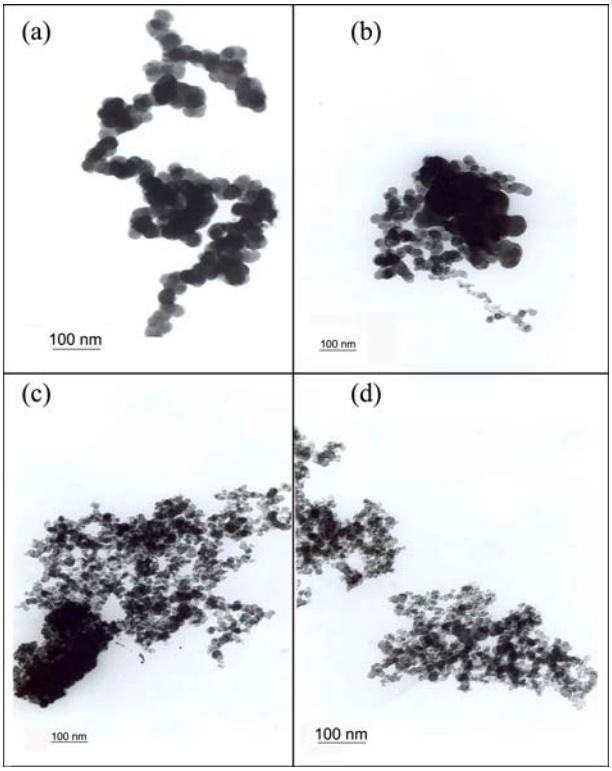

Figure 5. TEM images of TiO_2 (a) pure, (b) 0.4% W-doped, (c) 2% W-doped, and (d) 4% W-doped nano TiO_2.

TiO_2 framework. The particle size distribution obtained from the analysis of TEM images is also shown in Figure 6. Pure nanocrystalline TiO_2, were largely distributed around 23-40 nm. On the other hand, the W (2%)-TiO_2, was sharply distributed around 12-17 nm. Indeed, more than 75% were around 12-17 nm. In addition, W (4%)-TiO_2 was distributed around 6-23 nm and almost 30% were smaller than 10 nm.

FT-IR Studies. IR spectra of pure TiO_2 and W-doped TiO_2 are shown in Figure 7. The absorption bands in the region between 3300-3400 and 1620-1630 cm^{-1} show peaks corresponding to the stretching vibrations of O-H and bending

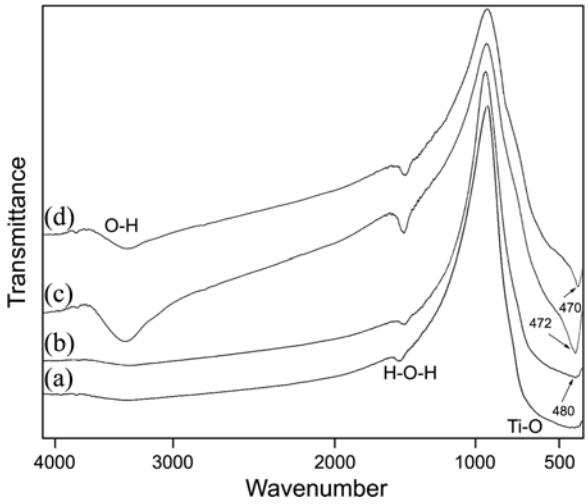

Figure 7. FT-IR spectra of (a) pure, (b) 0.4% W-doped, (c) 2% W-doped, and (d) 4% W-doped nano TiO_2.

vibrations of adsorbed water molecules, respectively. The band at 450-800 cm^{-1} assigned to Ti-O-Ti was observed over all samples.[28] In addition, the peaks corresponding to C-H bending (1360-1470 cm^{-1}) and the other organic molecules were not observed.

Photocatalytic Degradation of 4-NP.

Optimum Amount of Tungsten on the Degradation of 4-NP: To investigate the photocatalytic activity of the W-doped TiO_2 and find out the optimum amount of W-doping, a series of degradation reactions on 4-NP were carried out by using different W-doped TiO_2 photocatalysts. The results are shown in Figure 8. It demonstrates that all the W-doped TiO_2 samples are better than the pure in photodegradation efficiency and the 2.0 mol % W-doped TiO_2 photocatalyst has the highest efficiency. It is clear that particle size is important to rate degradation of pollutants. As the size is reduced the particle surface area will increase. Based on this fact the 2 mol % W-doped sample has larger surface area by a factor of two compared to the pure anatase, and this factor could enhance the activity of catalyst. Indeed, the doping

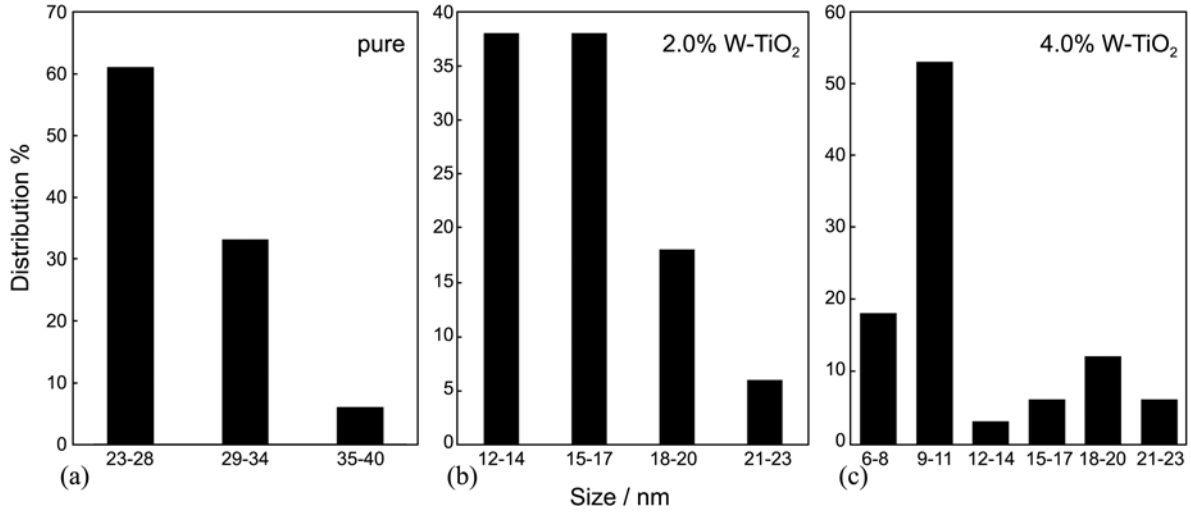

Figure 6. Particle distribution of synthesized samples: (a) pure, (b) 2% W-doped, and (c) 4% W-doped TiO_2.

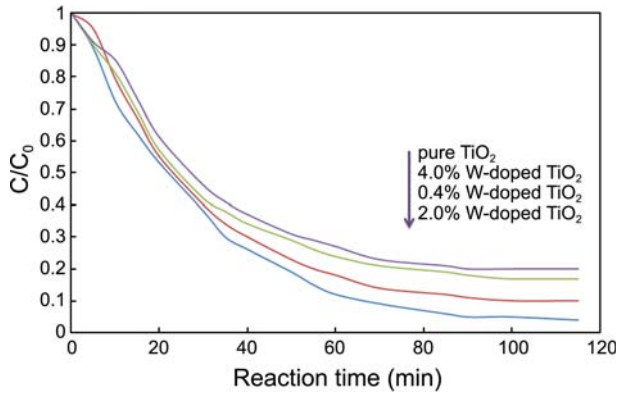

Figure 8. The effect of W-doped amount on 4-NP degradation reaction (initial concentration of the 4-NP = 10 mg L^{-1} and photocatalyst = 35 mg).

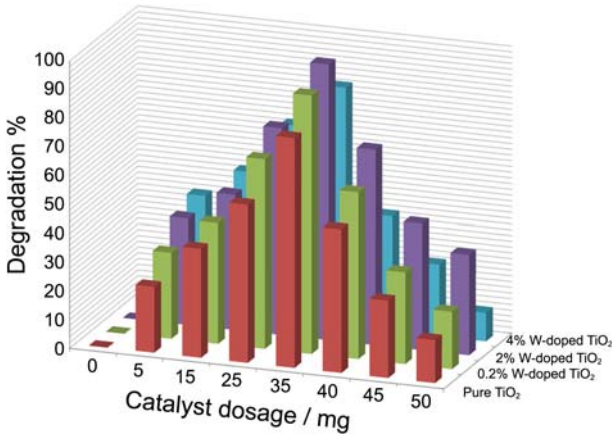

Figure 10. The effect of TiO_2 dosage on the degradation (initial concentration of the 4-NP = 10 ppm).

substitution of Ti atoms by W atoms with higher-valence cations leads to an alteration of the electronic structure of the nano pure TiO_2, which assists the charge separation efficiency. Therefore, W acts as an effective separation center for electrons and holes. The photo-generated charge carriers can be transferred into different surface sites where they will react with adsorbed 4-NP and enhance photocatalytic activity. Thus, the photoexcited electrons in the conduction band can be accepted by W^{6+} ions. On the other hand, too high-loaded W would act as recombination centers.

Effect of Initial Concentration of 4-NP. Different concentration profiles were observed during the degradation of different initial concentrations. Experimental results are shown in Figure 9. Since the pollutant concentration is an important parameter in water treatment, the effect of the initial concentration of 4-NP on the photocatalytic degradation rate was investigated over the concentration range of 10-120 ppm. The results show that the degradation depends on the initial 4-NP concentration. The degree of photodegradation decreased with increasing of initial concentration of 4-NP. The degradation rate is directly proportional to the formation of hydroxyl radicals (˙OH) on the catalyst surface. It can be pointed out that, due to the redox potentials of the electron-hole pair, H_2O_2 can theoretically be formed

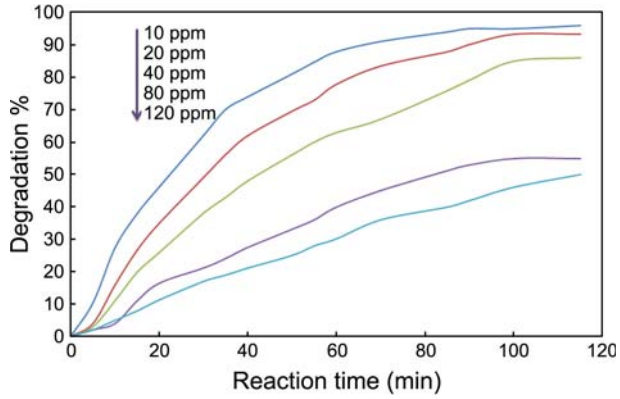

Figure 9. The effect of initial concentration of 4-NP on the photocatalytic degradation rate (photocatalyst = 35 mg).

via two different pathways in the presence of pure oxygen gas as follows:

$$O_2 + 2e_{cb}^- + H^+ \rightarrow H_2O_2$$

$$2H_2O + 2h_{vb}^+ \rightarrow H_2O_2 + 2H^+$$

Then hydroxyl radicals are produced during UV-light dissociation of H_2O_2 ($H_2O_2 + hv \rightarrow 2$ ˙OH). When initial concentration increase, more organic substances are absorbed on the surface of TiO_2. Therefore, there are only a fewer active sites for adsorption of hydroxyl ions so the generation of hydroxyl radicals will be reduced. As it can be seen from the values given in Figure 9, degradation percent decreases from 96 to 50%, during 115 min, when the initial 4-NP concentration increases from 10 to120 ppm.

Effect of Photocatalyst Dosage. The effect of catalyst loading on degradation of 4-NP was investigated using TiO_2 from 0 to 50 mg keeping another parameters constant. The results are shown in Figure 10. Experiments performed with different concentrations of TiO_2 nanocrystalline showed that without catalyst, the degradation of 4-NP is insignificant. The photodegradation efficiency increased with an increase in pure and tungsten doped TiO_2 nanocrystalline concentration up to a certain point then begins to decrease gradually. Maximum degradation was obtained at 35 mg. Indeed, this limiting value mainly results from following two factors: (a) aggregation of TiO_2 particles at high concentrations, causing a decrease in the number of surface active sites, and (b) increase in opacity and light scattering of TiO_2 particles at high concentration leading to a decrease in the passage of irradiation through the sample. The total active surface area increases with increasing catalyst dosage. Since the most effective decomposition of 4-NP was observed with 35 mg of TiO_2 nanocrystalline, the other experiments were performed in this concentration of TiO_2 nanocrystalline.

Conclusions

Compared to other methods, TiO_2 nanoparticles were prepared using microwave irradiation as an easy and very fast

method. Despite the conventional heating treatment, microwave treatment results in crystal samples without increasing the size. The incorporation of W in TiO_2 led to small grain size and high band gap values. The particle size of nano TiO_2 decreased with an increase in doping tungsten. Titanium alkoxo-acetates can be formed by the reaction of acetic acid with titanium alkoxides. Then, the hydrolysis rate of titanium alkoxo could be reduced. After adding water, the coordinated acetate is partially replaced by the hydroxyl group of water. Microwave process was employed following the sol to prepare the TiO_2. The photocatalytic activity was tested on the degradation of 4-NP. The results show that the photocatalytic activity of the W-doped TiO_2 photocatalyst is much higher than that of pure TiO_2, and the optimum percentage of W doped is 2.0 mol %.

Acknowledgments. The authors are grateful to the Research Council of Guilan University for the partial support of this study.

References

1. Palmisano, V.; Augugliaro, L.; Sclafani, A.; Schiavello, M. *J. Phys. Chem*. **1988**, *92*, 6710.
2. Luo, H.; Takata, T.; Lee, Y.; Zhao, J.; Domen, K.; Yan, Y. *Chem. Mater*. **2004**, *16*, 846.
3. Fox, M. A.; Dulay, M. T. *Chem. Rev.* **1993**, *93*, 341.
4. Kominami, H.; Kato, J.-I.; Murakami, S.-Y.; Kera, Y.; Inoue, M.; Inui, T.; Ohtani, B. *J. Mol. Catal. A Chem.* **1999**, *144*, 165.
5. Rao, M. V.; Rajeshwar, K.; Pai Verneker, V. R.; DuBow, J. *J. Phys. Chem.* **1980**, *84*, 1987.
6. Scolan, A.; Sanchez, C. *Chem. Mater.* **1998**, *10*, 3217.
7. Wu, M.; Long, J.; Huang, A.; Luo, Y.; Feng, Sh.; Xu, R. *Langmuir* **1999**, *15*, 8822.
8. Wu, M.; Lin, G.; Chen, D.; Wang, G.; He, D.; Feng, S.; Xu, R. *Chem. Mater.* **2002**, *14*, 1974.
9. Yang, S.; Gao, L. *J. Am. Ceram. Soc.* **2005**, *88*, 968.
10. Zhu, H. Y.; Lan, Y.; Gao, X. P.; Ringer, S. P.; Zheng, Z. F.; Song, D. Y.; Zhao, J. C. *J. Am. Chem. Soc.* **2005**, *127*, 6730.
11. Colon, G.; Hidalgo, M. C.; Navio, J. A. *Catal. Today* **2002**, *76*, 91.
12. Ozer, R. R.; Ferry, J. L. *Environ. Sci. Technol.* **2001**, *35*, 3242.
13. Hoffmann, M. R.; Martin, S. T.; Choi, W.; Bahnemann, D. *Chem. Rev.* **1995**, *95*, 69.
14. Fernández-García, M.; Martínez-Arias, A.; Hanson, J. C.; Rodriguez, J. A. *Chem. Rev.* **2004**, *104*, 4063.
15. Yamamoto, T.; Wada, Y.; Yin, H.; Sakata, T.; Mori, H.; Yanagida, S. *Chem. Lett.* **2002**, 964.
16. Hart, J. N.; Cervini, R.; Cheng, Y.-B.; Simon, G. P.; Spiccia, L. *Sol. Energy Mater. Sol. Cells* **2004**, *84*, 135.
17. Komarneni, S.; Rajha, R. K.; Katsuki, H. *Mat. Chem. Phys.* **1999**, *61*, 50.
18. Tian, H.; Ma, J.; Li, K.; Li, *J. Mater. Chem. Phys.* **2008**, *112*, 47.
19. Fallah Shojaie, A.; Loghmani, M. H. *Chem. Eng. J.* **2010**, *157*, 263.
20. Fallah Moafi, H.; Fallah Shojaie, A.; Zanjanchi, M. A. *Appl. Surf. Sci.* **2010**, *256*, 4310.
21. Fallah Moafi, H.; Fallah Shojaie, A.; Zanjanchi, M. A. *Chem. Eng. J.* **2011**, *166*, 413.
22. Rezvani, M. A.; Fallah Shojaie, A.; Loghmani, M. H. *Catal. Commun.* **2012**, *25*, 36.
23. Nair, J.; Nair, P.; Mizukami, F.; Oosawa, Y.; Okubo, T. *Mater. Res. Bull.* **1999**, *34*, 1275.
24. Hsien, Y. H.; Chang, C. F.; Chen, Y. H.; Cheng, S. *Appl. Catal. B: Environ.* **2001**, *31*, 241.
25. Ohsaka, T.; Izumi, F.; Fujiki, Y. *J. Raman Spectroscopy* **1978**, *7*, 321.
26. Chan, S. S.; Wachs, I. E.; Murrell, L. L.; Wang, L.; Hall, W. K. *J. Phys. Chem.* **1984**, *88*, 5831.
27. Daniel, M. F.; Desbat, B.; Lassegues, J.; Gerand, B.; Figlarz, M. *J. Solid State Chem.* **1987**, *67*, 235.
28. Furusawa, T.; Honda, K.; Ukaji, E.; Sato, M.; Suzuki, N. *Mater. Res. Bull.* **2008**, *43*, 946.